Contrastive Bi-Projector for Unsupervised Domain Adaption

Lin-Chieh Huang, Hung-Hsu Tsai

***Abstract*—This paper proposes a novel unsupervised domain adaption (UDA) method based on contrastive bi-projector (CBP), which can improve the existing UDA methods. It is called CBPUDA here, which effectively promotes the feature extractors (FEs) to reduce the generation of ambiguous features for classification and domain adaption. The CBP differs from traditional bi-classifier-based methods at that these two classifiers are replaced with two projectors of performing a mapping from the input feature to two distinct features. These two projectors and the FEs in the CBPUDA can be trained adversarially to obtain more refined decision boundaries so that it can possess powerful classification performance. Two properties of the proposed loss function are analyzed here. The first property is to derive an upper bound of joint prediction entropy, which is used to form the proposed loss function, contrastive discrepancy (CD) loss. The CD loss takes the advantages of the contrastive learning and the bi-classifier. The second property is to analyze the gradient of the CD loss and then overcome the drawback of the CD loss. The result of the second property is utilized in the development of the gradient scaling (GS) scheme in this paper. The GS scheme can be exploited to tackle the unstable problem of the CD loss because training the CBPUDA requires using contrastive learning and adversarial learning at the same time. Therefore, using the CD loss with the GS scheme overcomes the problem mentioned above to make features more compact for intra-class and distinguishable for inter-class. Experimental results express that the CBPUDA is superior to conventional UDA methods under consideration in this paper for UDA and fine-grained UDA tasks.**

***Index Terms*—Unsupervised domain adaption, transfer learning, adversarial learning, bi-classifer, contrastive learning.**

I. INTRODUCTION

RECENTLY, the deep learning on real-world applications has significant success due to having massive labeled data [1]. However, the collected data may contain a lot of noises or outliers. Therefore, training models requires huge hand-craft annotations for labeling collected data. It is very time-consuming. Thankfully, recent researches on unsupervised domain adaption (UDA) techniques are growing fast and tackle many real-world problems without requiring huge number of labels, such as image classification [1-23], image segmentation [24-27] etc. The UDA models can be easily built using given labeled data. Then, they are capable of effectively transferring the knowledge on labeled data to generalize their discriminability on unlabeled complex data.

The goal of the UDA is to align two different domains where they share with the same label spaces but their distributions are not identical. Usually, domains with labels and without labels are called the source domain and the target domain, respectively. However, the main research challenge of designing the UDA is that the alignment is not guarantee to have great discriminability among classes of the target domain after transferring knowledge from the source domain to the target domain. Although these two domains overlap in the feature space, the domain shift between these two domains causes poor performance on categorical recognition due to a large domain gap.

Many UDA schemes aim to mitigate the domain shift. Deep adaption network (DAN) minimizes the feature distance between source and target domains using the mean-maximum discrepancy (MMD) and aligns features in each layer of the FE in DAN [1]. Domain-adversarial neural network (DANN) leverages the mechanism of GAN [32] to generate domain-invariant features of two domains where the FE and the domain classifier in DANN are updated by using the min-max optimization [2]. A variational autoencoder-like framework is proposed to align the features of two domains in the same normal distribution and then map the normal distribution to their original distributions [3]. However, the above schemes suffer from the problem that they cannot class-wisely align features between source and target domain. Thus, their produced features are lack of intra-class compactness and inter-class separability. Recently, most of articles propose the class-conditioned UDA to tackle the problem mentioned above. Deep Subdomain Adaption Network modifies the MMD to Local MMD (LMMD) which is class-conditioned [4]. Moreover, Adversarial Tight Match (ATM) is proposed to promote the LMMD [5]. Conditional Adversarial Network (CDAN) utilizes the multilinear-map property in the design of the domain classifier using class information to get a huge progress of intra-class compactness and inter-class separability [6]. Metric learning-based methods strengthen the relationship between positive and negative features to make the feature clusters more distinguishable. Cycle-consistent-based schemes assume the centers of target features of classes can be used to forecast the categories of source features [7, 8]. Another branch of the kind of class-conditioned UDA is called the bi-

This work is partially supported by NSTC 111-2634-F-005-001 - project Smart Sustainable New Agriculture Research Center (SMARTer), NSTC 112-2221-E-005-082, and the "Innovative Center on Sustainable Negative-Carbon Resources" from the Featured Areas Research Center Program within the framework of the Higher Education Sprout Project by MOE in Taiwan. *(Corresponding author: Hung-Hsu Tsai).*

Lin-Chieh Huang is with the Institute of Data Science & Information Computing, National Chung Hsing University, 402, Taichung, Taiwan (e-mail: tom99763@gmail.com).

Hung-Hsu Tsai is with the Institute of Data Science & Information Computing, National Chung Hsing University, 402, Taichung, Taiwan (e-mail: afhmthh@nchu.edu.tw).

classifier method. It performs the UDA by, first, maximizing the disagreement of the predictions of two classifiers and then minimizing the disagreement of the predictions of two classifiers with the features generated by the FE. The first bi-classifier method is called Maximum Class Discrepancy (MCD) for UDA. MCD evaluates the disagreement between two classifiers by l_1 distance [9]. Bi-Classifier Determinacy Maximization (BCDM) mitigates the ambiguous predictions in MCD via assessing the determinacy discrepancy between two classifiers [10]. JD-MMD combines MMD, bi-classifier and domain classifier for peforming UDA [11]. Multi-Representation Adaptation Network (MRAN) is developed a to learn multi-representation of an image [12], which can carry out more refined domain alignment by using multiple features. Stochastic Classifiers (STAR) approximate infinite classifiers by learning the weights of a bi-classifier. These weights follow a gaussian distribution. Then, STAR can improve the performance of conventional bi-classifier methods [13]. Dual F-Certainty Maximization (DFCM) minimizes the F-norm of the prediction of one classifier to degrade its prediction on target domain and enhance the ability of another classifier on target domain [14].

However, conventional bi-classifier-based UDA schemes suffer from generating ambiguous features. This leads to getting poor classification performance. In Fig. 1, blue solid triangle and square represent the features of two classes in source domain. Moreover, red solid triangle and square stand for the features of two classes in target domain. In Fig. 1 (a), the BCDM makes the FE generate the unreliable features (represented by red hollow triangle and square). Those unreliable features are incorrectly judged by the two classifiers. The figure in right bottom of Fig. 1 (a) illustrates the BCDM has acceptable UDA result but still obtaining poor classification. The reason is that traditional UDA methods are based on the prototypes without involving the relationship between features. This motivates us to propose the contrastive bi-projector (CBP) to deal with the ambiguous problem mentioned above. Fig. 1 (b) depicts how the CBP works well in generating separable clusters of features. Two projectors in the CBP map the features the FE produces into the hypersphere. Then, the distances between the features and the prototypes (represented by yellow solid triangle and square in Fig. 1 (b)) are computed. Subsequently, the distances are used to calculate the CD loss. More specifically, the behavior of the CD loss in the CBPUDA can be described in the following. First, the pseudo-labels of unreliable features of a class in Fig. 1 (b) are assigned by a nearest prototype. Second, features in the same class are pulled to approach their corresponding prototype. Meanwhile, they are pushed away from the features which are in different classes. Third, to avoid misassignment of pseudo-labels, the CBP rejects the pushing and pulling operations in the second step by the adversarial training. Finally, the FE in the CBPUDA can produce powerfully discriminative features and then improve the classification performance of the conventional UDA methods. The figure in the right bottom of Fig. 1 (b) show that features generated by the CBPUDA are well classified. The main contributions of this paper can be summarized in the following.

- A novel loss function, the CD loss, is proposed in this article for improving existing UDA methods, which inherits the advantages of the characteristics of contrastive learning and bi-classifier.
- The GS scheme is devised, which can effectively address the problem of the CD loss and stabilize the training of the CBPUDA. The experiment results demonstrate that the GS can boost huge performance while setting less temperature coefficient in the CD loss.
- The success of developing the contrastive loss as the loss function for adversarial training is a main contribution of this paper.

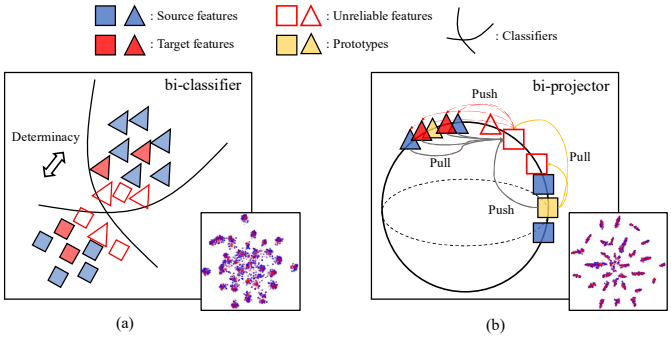

Fig. 1. Comparing the schemes between (a) BCDM and (b) CBPUDA.

II. Related Works

A. Unsupervised Domain Adaption

Unsupervised domain adaption (UDA) methods can be mainly grouped into three categories: adversarial-based, metric-based and bi-classifier-based. First, the framework of adversarial-based UDA is similar to generative adversarial network (GAN) [32]. It consists of three components, the feature extractor, the classifier, and the discriminator. The core mechanism to align features is to confuse the discriminator to distinguish which domain the features belong to. The article first proposes this kind of principles to implement the UDA tasks [2]. The gradient reversal method is developed to conduct the min-max optimization, where the reverse-direction gradients are used to update the weights of the FE. The CDAN is proposed in the work [6]. The input features of the discriminator of the CDAN are the outer product between the feature vectors the FE generates and the prediction vectors the classifier outputs. This scheme helps the discriminator to perform domain discrimination not only involving the domains but also the classes. The DM-ADA leverages the Mix-up augmentation to enhance the relationship between a linear combination of images and a linear combination of features [15]. The chief idea is to exploit the interpolation between source and target images, which also exists in their features. It turns out that the FE in the DM-ADA can generate smooth features to get satisfied performance.

Most of metric-based UDA methods employ the MMD to

measure the distance between source and target feature distributions. The article leverages the MMD to minimize the distribution gap between source and target features [1]. The LMMD computes the class-wise distance therefore it can deal with more refined measurement [4]. Furthermore, another work proposes the density divergence to replace the LMMD [5]. This way gets better performance than the LMMD. Some metric-based UDA schemes utilize special mechanisms of adapting source and target features. The cycle-consistent loss is developed in [7] and [8]. The target features is also capable of forecasting the class the source features belong to if the source features can be utilized to predict the class the target features belong to. The triplet loss for the UDA is developed to improve the relationship between classes and features [16]. Basically, the triplet loss can achieve that the positive features are closer to the anchors and the negative features are further to the anchors. A scheme proposes a strategy, initializing the centers by averaging source features and using k-means algorithm on target features [17]. By this strategy, the pseudo-labels can be predicted more precisely. It also improves existed metric-based methods due to the requirements of getting accurate pseudo-labels for the UDA.

Bi-classifier-based UDA methods share similarities with adversarial-based UDA techniques as they also utilize adversarial training to adapt target features to source features. In this approach, two classifiers (bi-classifier) serve as discriminators, measuring the domain discrepancy based on the classes they predict. For instance, the MCD employs the l_1 loss to evaluate prediction differences. Its experimental results have shown comparable performance on some UDA tasks [9]. To address the issue of the MCD generating unconfident features, the BCDM introduces the classifier determinacy disparity (CDD) metric, which computes cross predictions between these two classifiers [10]. This metric aims at improving feature confidence and enhancing overall performance. An alternative method, the stochastic classifiers (STAR) approach, leverages the concept of ensemble learning by approximating an infinite number of classifiers using a Gaussian distribution to model the distribution of weights of the classifiers [13]. This technique has promising results in certain scenarios. Furthermore, the uneven bi-classifier is that one classifier prioritizes accurate predictions while the other is constrained to predict only classes from the target domain. It has proven to be a highly effective scheme in outperforming existing UDA methods [14].

B. Contrastive Learning

The CL can be used to effectively train the FE which generates highly distinguishable features. The core idea of the CL involves comparing an anchor sample with a positive sample and a set of negative samples. For instance, the contrastive predictive coding (CPC) scheme, which is introduced in [18], trains a network to predict future patches of images using the InfoNCE loss to memorize dependencies between current and future patches. Building upon this, an article proposes an unsupervised pretraining framework based on InfoNCE loss for various downstream tasks [19]. Here, the positive sample is regarded as an augmented anchor image while the negative samples consist of all other images except the anchor image. Moreover, another article presents a supervised CL method that demonstrates high performance on downstream tasks when labels are in advance available [20]. In the research fields of GANs, several articles explore that the CL is used to boost generative task performance. An approach, the patch-wise InfoNCE proposed in [21], utilizes a patch in the generated image as the anchor sample while a corresponding patch from the input image is taken as the positive sample and a set of other patches from the input image is regarded as negative samples. This approach aids in finding semantic correspondence between input and generated images. To address the mode collapse problem in conditional generation tasks, two papers present an additional CL task for strengthening the discriminator in GANs [22, 23].

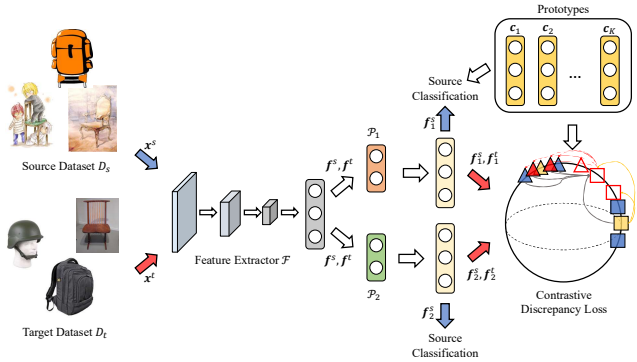

Fig. 2. The framework of the CBPUDA.

III. THE CBPUDA METHOD

Fig. 2 shows the framework of the CBPUDA. First, source image $\boldsymbol{x}^s$ and target image $\boldsymbol{x}^t$ are respectively selected from source dataset D_s and target dataset D_t. Second, $\boldsymbol{x}^s$ and $\boldsymbol{x}^t$ are fed into feature extractor $\mathcal{F}$ and then $\mathcal{F}$ produces source feature $\boldsymbol{f}^s$ and target feature $\boldsymbol{f}^t$, respectively. Third, two projectors $\mathcal{P}_1$ and $\mathcal{P}_2$ produce $\boldsymbol{f}^s$ and $\boldsymbol{f}^t$ to form two feature pairs, $(\boldsymbol{f}_1^s, \boldsymbol{f}_2^s)$ and $(\boldsymbol{f}_1^t, \boldsymbol{f}_2^t)$. Forth, the classification loss is computed by $(\boldsymbol{f}_1^s, \boldsymbol{f}_2^s)$ and prototypes $\{\boldsymbol{c}_k\}_{k=1}^K$. Note that $\boldsymbol{c}_k$ denotes the kth prototype of class k. Finally, $(\boldsymbol{f}_1^s, \boldsymbol{f}_2^s)$ and $(\boldsymbol{f}_1^t, \boldsymbol{f}_2^t)$ are used in computing the contrastive discrepancy loss (ℓ_{cd}) which is utilized in adapting the target features to the source features. Note that a projector $\mathcal{P} \in \{\mathcal{P}_1, \mathcal{P}_2\}$ and a set of prototypes $\{\boldsymbol{c}_k\}_{k=1}^K$ are regarded as a classifier $\mathcal{C}$. That is, $\mathcal{C}$ is constituted with $\mathcal{P}$ and $\{\boldsymbol{c}_k\}_{k=1}^K$.

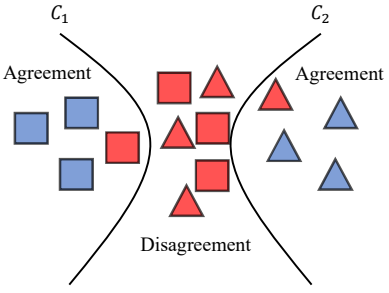

Fig. 3. The behavior of the bi-classifier for UDA.

A. Preliminary

Let $D_s = \{(\boldsymbol{x}_i^s, y_i^s)\}_{i=1}^{N_s}$ and $D_t = \{\boldsymbol{x}_i^t\}_{i=1}^{N_t}$ be the labeled source domain dataset and the unlabeled target domain dataset, respectively. Here $\boldsymbol{x}_i^s$, $\boldsymbol{x}_i^t$ and y_i^s denote a source image, a target image, and the corresponding label of $\boldsymbol{x}_i^s$, respectively. The goal of the UDA is to simultaneously train an FE, $\mathcal{F}$, and a classifier, $\mathcal{C}$, on D_s and then transfer $\mathcal{C}$'s discrimination ability to D_t. $\mathcal{F}$ is expected to map the source and the target domains to the same feature distribution. Meanwhile, $\mathcal{C}$ may have a great discriminative ability on both D_s and D_t.

The bi-classifier is one kind of traditional UDA methods [9, 10, 13, 14]. The main assumption of the bi-classifier is that two classifiers have the same prediction results for the target features. Here, it is so called two domains are undistinguishable. Fig. 3 displays the behavior of the bi-classifier for the UDA. Two classifiers $\mathcal{C}_1$ and $\mathcal{C}_2$ are represented by two curves, their corresponding decision boundaries for two classes (triangles and rectangles). They have an agreement on source features but a disagreement on the target features (colored by red) in the middle. $\mathcal{C}_1$ classifies them as triangles colored by red. Instead, $\mathcal{C}_2$ classifies them as rectangle colored by red. The goal of the bi-classifier is to train $\mathcal{F}$ so that it can generate features to make the agreement between $\mathcal{C}_1$ and $\mathcal{C}_2$. Once the generated features follow this goal, the recognition abilities of $\mathcal{C}_1$ and $\mathcal{C}_2$ on the source domain can be transferred to that of the target domain. From the above descriptions, the loss functions of training the bi-classifier can be formulated as the classification loss ℓ_{cls} in (1) and the discrepancy loss ℓ_{dis} in (2).

$$\min_{\mathcal{F},\mathcal{C}_1,\mathcal{C}_2}\left\{\ell_{cls} = \mathbb{E}_{x^s\sim D_s}[-\log p_1(\boldsymbol{x}^s) - \log p_2(\boldsymbol{x}^s)]\right\} \quad (1)$$

$$\min_{\mathcal{F}}\max_{\mathcal{C}_1,\mathcal{C}_2}\left\{\ell_{dis} = \mathbb{E}_{\boldsymbol{x}^t\sim D_t}\left[d\left(p_1(\boldsymbol{x}^t), p_2(\boldsymbol{x}^t)\right)\right]\right\} \quad (2)$$

where $p_i(\boldsymbol{x}) = \mathcal{C}_i\left(\mathcal{F}(\boldsymbol{x})\right)$, for each i. The distance $d(\cdot,\cdot)$ measures the discrepancy between $\mathcal{C}_1$ and $\mathcal{C}_2$.

B. Contrastive Discrepancy Maximization

l_1 distance is used to measure the discrepancy between two classifiers in the MCD [9]. However, the article finds out that using l_1 to optimize these classifiers lead to ambiguous predictions [10]. Therefore, the joint entropy is involved in the design of the BCDM, which can be defined in (3). (Ignoring the case of $p_1 = p_2$ in the BCDM).

$$H(p_1, p_2) = \mathbb{E}_{x^t\sim D_t}[-\log p_1(y|\boldsymbol{x}^t)p_2(y|\boldsymbol{x}^t)] \quad (3)$$

However, using the prediction of two classifiers to estimate $H(p_1, p_2)$ does not consider the dependencies between the features. This results in that the generated features are not powerfully discriminative because the weights of $\mathcal{C}_1$ and $\mathcal{C}_2$ only contain the relationship between features and the feature centers but without relationship among features. To improve the measurement of the discrepancy between two classifiers, this paper proposes a novel loss function according to the joint entropy, which has both of two relationships mentioned above. Let the weights of a classifier be $\boldsymbol{c} = [\boldsymbol{c}_1, \dots, \boldsymbol{c}_K]^T \in \mathbb{R}^{K\times d}$ and the feature vector be $\boldsymbol{f} = [f_1, \dots, f_d] \in \mathbb{R}^d$, where K and d denote the number of classes and the dimension of the feature vector, respectively. The *logit*, outputs of a classifier, can be rewritten in (4).

$$\begin{aligned} logit &= \begin{bmatrix} c_{11} & \cdots & c_{1d} \\ \vdots & \ddots & \vdots \\ c_{K1} & \cdots & c_{Kd} \end{bmatrix}\begin{bmatrix} f_1 \\ \vdots \\ f_d \end{bmatrix} = [\boldsymbol{c}_1 \quad \dots \quad \boldsymbol{c}_K]^T \begin{bmatrix} f_1 \\ \vdots \\ f_d \end{bmatrix} \\ &= [\boldsymbol{c}_1\boldsymbol{f} \quad \dots \quad \boldsymbol{c}_K\boldsymbol{f}]^T \end{aligned} \quad (4)$$

Observing (4), the *logit* can be treated as the unnormalized similarities between $\boldsymbol{c}_k$ and $\boldsymbol{f}$, for $k = 1$ to K. Therefore, $\boldsymbol{c}_1, \dots, \boldsymbol{c}_K$ are regarded as the *prototypes*, which represent the centers of the classes. $\boldsymbol{c}_k$ can be defined as the conditional expectation in (5).

$$\boldsymbol{c}_k = \mathbb{E}[\boldsymbol{f}|y = k] \quad (5)$$

In the design of the CBPUDA, a set of weights of $\mathcal{C}$ performs the expectation in (5). In contrast, an article uses the average of feature vectors in a class to realize the expectation in (5) [17]. Therefore, the soft-max function can be written by (6),

$$p_i(y = k|\boldsymbol{x}) = \frac{\exp(\boldsymbol{f}_i^T\boldsymbol{c}_k)}{\sum_{k'=1}^{K}\exp(\boldsymbol{f}_i^T\boldsymbol{c}_{k'})} \quad (6)$$

where p_i is the prediction of the ith classifier. Using (3), (5) and (6), **Property I** can be derived and contrastive discrepancy loss ℓ_{cd} can be formulated in (7). More details of the derivations can be found in **Appendix A**.

Property I. $H(p_1, p_2) \le \mathbb{E}_{\boldsymbol{x}^t\sim D_t, \{\boldsymbol{x}_j\}_{j=1}^{M}\sim D_s\cup D_t}\left[-\log\frac{e^{\boldsymbol{f}_1^T\boldsymbol{c}_{k_1}+\boldsymbol{f}_2^T\boldsymbol{c}_{k_2}}}{e^{\boldsymbol{f}_1^T\boldsymbol{c}_{k_1}+\boldsymbol{f}_2^T\boldsymbol{c}_{k_2}}+\sum_{j=1}^{M}\sum_{j'=1}^{M}1_{y^{(j)}\neq k_1, y^{(j')}\neq k_2}e^{\boldsymbol{f}_1^T\boldsymbol{f}^{(j)}+\boldsymbol{f}_2^T\boldsymbol{f}^{(j')}}}\right]$

$$\ell_{cd} = \mathbb{E}_{x^t\sim D_t, \{x^{(j)}\}_{j=1}^{M}\sim D_s\cup D_t}\left[-\log\frac{e^{(\boldsymbol{f}_1^T\boldsymbol{c}_{k_1}+\boldsymbol{f}_2^T\boldsymbol{c}_{k_2})/\tau}}{e^{(\boldsymbol{f}_1^T\boldsymbol{c}_{k_1}+\boldsymbol{f}_2^T\boldsymbol{c}_{k_2})/\tau}+\sum_{j=1}^{M}\sum_{j'=1}^{M}1_{y^{(j)}\neq k_1, y^{(j')}\neq k_2}e^{\left(\boldsymbol{f}_1^T\boldsymbol{f}^{(j)}+\boldsymbol{f}_2^T\boldsymbol{f}^{(j')}\right)/\tau}}\right] \quad (7)$$

where $M = N_s + N_t$, τ and $\{\boldsymbol{x}^{(j)}\}_{j=1}^{M}$ express the number of negative samples, the temperature coefficient, and a set of negative samples, respectively. To reduce computational complexity for (7), this paper adopts the nearest c_{k_i} for f_i

rather than computing the average of $\{\boldsymbol{c}_{k_i}\}_{k_i=1}^{K}$. Comparing (7) with (3), ℓ_{cd} in (7) leverages more information between anchor features, f_1 and f_2, and negative features, $\{\boldsymbol{f}^{(j)}\}_{j=1}^{M}$ for $\{\boldsymbol{x}^{(j)}\}_{j=1}^{M}$. Additionally, the indicator function, $1_{y^{(j)}\neq k_1, y^{(j')}\neq k_2}$, is zero when these two classifiers have predictions, $y^{(j)}=k_1$ and $y^{(j')}=k_2$. More specifically, the classes, k_1 and k_2, of anchor features, $\boldsymbol{f}_1$ and $\boldsymbol{f}_2$ are respectively identical to the classes, $y^{(j)}$ and $y^{(j')}$, negative samples, $\boldsymbol{f}^{(j)}$ and $\boldsymbol{f}^{(j')}$, belong to. This way differs from the conventional bi-classifier loss functions at calculating ℓ_{cd} using the target features and the source features instead of only using target features in loss computations during domain adaption [9, 10, 13, 14]. Consequently, utilizing (7) in the design of the loss function d in (2) can obtain better performance than that of conventional bi-classifier methods. Several articles address the conditional GAN, whose loss functions are akin to ℓ_{cd} [22, 23]. Their models can judge not only realism among the generated images but also the similarities among corresponding features. These methods can be employed to solve the mode collapse problem in the ACGAN [24]. The problem is that some contents of the generated images are repeatedly appear because of just using prototypes in the design of traditional classifiers to perform classification.

The loss functions of the CBPUDA can be specified in (8) and (9) via modifying the loss functions in (1) and (2).

$$\min_{\mathcal{F},\mathcal{P}_1,\mathcal{P}_2,\{\boldsymbol{c}_k\}_{k=1}^{K}} \ell_{cls} \tag{8}$$

$$\min_{\mathcal{F}} \max_{\mathcal{P}_1,\mathcal{P}_2,\{\boldsymbol{c}_k\}_{k=1}^{K}} \ell_{cd} \tag{9}$$

Furthermore, the optimization of ℓ_{cd} can figure out from an information-theoretic perspective. Let the mutual information between $\mathcal{P}_1$ and $\mathcal{P}_2$ denote $I(p_1;p_2)$. By the definition of mutual information, it can be formulated as $I(p_1;p_2)=H(p_1)+H(p_2)-H(p_1,p_2)$. Utilizing **Property I**, we have $I(p_1;p_2)\geq H(p_1)+H(p_2)-\ell_{cd}\triangleq I'(p_1;p_2)$. This implies that the mutual information between $\mathcal{P}_1$ and $\mathcal{P}_2$ is at least greater than $I'(p_1;p_2)$. Consequently, in (9), the minimization of ℓ_{cd} can be expressed as the maximization of $I'(p_1;p_2)$ with respect to $\mathcal{F}$. In other words, minimizing ℓ_{cd} is to encourage $\mathcal{F}$ to generate features that have more shared information between $\mathcal{P}_1$ and $\mathcal{P}_2$. It has the case of increasing lower bound of $I(p_1;p_2)$. The purpose of the way mentioned above is to enhance the performance of the CBPUDA by making the feature extractor to produce more informative and discriminative representations.

C. Stabilize Contrastive Discrepancy Loss Using Gradient Scaling

When optimizing ℓ_{cd} in (7), a finding is that if two projectors, $\mathcal{P}_1$ and $\mathcal{P}_2$, select the same prototype which is not ground truth, the CBPUDA gets poor performance and converges quickly. To investigate the reasons of the shortcomings, a derivation of gradients $\frac{\partial \ell_{cd}}{\partial \boldsymbol{f}_i}$ of ℓ_{cd} with respect to $\boldsymbol{f}_i$ can be found in (10), for $i\in\{1,2\}$.

$$\begin{aligned}
\frac{\partial \ell_{cd}}{\partial \boldsymbol{f}_i} &= -\frac{\boldsymbol{c}_{k_i}}{\tau}+\frac{1}{\tau}\left(\frac{\boldsymbol{c}_{k_i}e^{\frac{(\boldsymbol{f}_1^T\boldsymbol{c}_{k_1}+\boldsymbol{f}_2^T\boldsymbol{c}_{k_2})}{\tau}}+\sum_{j=1}^{M}\sum_{j'=1}^{M}1_{y^{(j)}\neq k_1,y^{(j')}\neq k_2}\boldsymbol{f}^{(j)}e^{\frac{(\boldsymbol{f}_1^T\boldsymbol{f}^{(j)}+\boldsymbol{f}_2^T\boldsymbol{f}^{(j')})}{\tau}}}{\boldsymbol{B}}\right)\\
&= -\frac{\boldsymbol{c}_{k_i}}{\tau}+\frac{1}{\tau\boldsymbol{B}}\left(\boldsymbol{c}_{k_i}e^{\frac{(\boldsymbol{f}_1^T\boldsymbol{c}_{k_1}+\boldsymbol{f}_2^T\boldsymbol{c}_{k_2})}{\tau}}+M\sum_{j=1}^{M}\boldsymbol{f}^{(j)}\sum_{j'=1}^{M}1_{y^{(j)}\neq k_1,y^{(j')}\neq k_2}e^{\frac{(\boldsymbol{f}_1^T\boldsymbol{f}^{(j)}+\boldsymbol{f}_2^T\boldsymbol{f}^{(j')})}{\tau}}\right)\\
&= -\frac{\boldsymbol{c}_{k_i}}{\tau}+\frac{1}{\tau B}\,\boldsymbol{c}_{k_i}e^{\frac{(\boldsymbol{f}_1^T\boldsymbol{c}_{k_1}+\boldsymbol{f}_2^T\boldsymbol{c}_{k_2})}{\tau}}+\frac{M}{\tau\boldsymbol{B}}\left(\sum_{j=1}^{M}\boldsymbol{f}^{(j)}\sum_{j'=1}^{M}1_{y^{(j)}\neq k_1,y^{(j')}\neq k_2}e^{\frac{(\boldsymbol{f}_1^T\boldsymbol{f}^{(j)}+\boldsymbol{f}_2^T\boldsymbol{f}^{(j')})}{\tau}}\right)\\
&= \frac{1}{\tau}\left(\boldsymbol{\alpha}\boldsymbol{c}_{k_i}+\sum_{j=1}^{M}\boldsymbol{\beta}^{(j)}\boldsymbol{f}^{(j)}\right)
\end{aligned} \tag{10}$$

where $\boldsymbol{\alpha}=-1+\frac{1}{\boldsymbol{B}}e^{\frac{(\boldsymbol{f}_1^T\boldsymbol{c}_{k_1}+\boldsymbol{f}_2^T\boldsymbol{c}_{k_2})}{\tau}}$, $\boldsymbol{\beta}^{(j)}=\frac{M}{\boldsymbol{B}}\sum_{j'=1}^{M}1_{y^{(j)}\neq k_1,y^{(j')}\neq k_2}e^{\frac{(\boldsymbol{f}_1^T\boldsymbol{f}^{(j)}+\boldsymbol{f}_2^T\boldsymbol{f}^{(j')})}{\tau}}$ and $\boldsymbol{B}=e^{\frac{(\boldsymbol{f}_1^T\boldsymbol{c}_{k_1}+\boldsymbol{f}_2^T\boldsymbol{c}_{k_2})}{\tau}}+\sum_{j=1}^{M}\sum_{j'=1}^{M}1_{y^{(j)}\neq k_1,y^{(j')}\neq k_2}e^{\frac{(\boldsymbol{f}_1^T\boldsymbol{f}^{(j)}+\boldsymbol{f}_2^T\boldsymbol{f}^{(j')})}{\tau}}$.

Observing (10), the value of $\frac{\partial \ell_{cd}}{\partial \boldsymbol{f}_i}$ is affected by three terms, τ, αc_{k_i} and $\sum_{j=1}^{M}\boldsymbol{\beta}^{(j)}f^{(j)}$. The second term can be interpreted as the scaling of the prototype. The third term can be referred to the linear combination of the negative samples. If $\mathcal{P}_1$ and $\mathcal{P}_2$ determine the same prototype, we have $\boldsymbol{c}_{k^*}=\boldsymbol{c}_{k_1}=\boldsymbol{c}_{k_2}$ and $\boldsymbol{f}^*=\boldsymbol{f}_1=\boldsymbol{f}_2$. Then, $\frac{\partial \ell_{cd}}{\partial \boldsymbol{f}^*}$ can be formulated by (11).

$$\frac{\partial \ell_{cd}}{\partial \boldsymbol{f}^*}=\frac{1}{\tau}\left(\boldsymbol{\alpha}^*\boldsymbol{c}_{k^*}+\sum_{j=1}^{M}\boldsymbol{\beta}^{*(j)}\boldsymbol{f}^{(j)}\right) \tag{11}$$

where $\boldsymbol{\alpha}^*=-1+\frac{1}{\boldsymbol{B}^*}e^{\frac{2\boldsymbol{f}^{*T}\boldsymbol{c}_{k^*}}{\tau}}$, $\boldsymbol{\beta}^{*(j)}=\frac{M}{\boldsymbol{B}^*}\sum_{j'=1}^{M}1_{y^{(j)}\neq k^*\neq y^{(j')}}e^{\frac{\boldsymbol{f}^{*T}(\boldsymbol{f}^{(j)}+\boldsymbol{f}^{(j')})}{\tau}}$ and $B^*=e^{\frac{2\boldsymbol{f}^{*T}\boldsymbol{c}_{k^*}}{\tau}}+$

$\sum_{j=1}^{M}\sum_{j'=1}^{M} 1_{y^{(j)}\neq k^*\neq y^{(j')}} e^{\frac{f^{*T}\left(f^{(j)}+f^{(j')}\right)}{\tau}}$. Subsequently, **Property II** can be derived. More details of the derivations can be found in **Appendix B**.

Property II. if $\frac{\partial \ell_{cd}}{\partial f^*}=0$, then $(\boldsymbol{\alpha}^*\boldsymbol{c}_{k^*})\left(\sum_{j=1}^{M}\boldsymbol{\beta}^{*(j)}\boldsymbol{f}^{(j)}\right)\neq 0$.

According to **Property II**, the case of $\frac{\partial \ell_{cd}}{\partial f^*}=0$ implies the condition $\boldsymbol{\alpha}^*\boldsymbol{c}_{k^*}+\sum_{j=1}^{M}\boldsymbol{\beta}^{*(j)}\boldsymbol{f}^{(j)}=0$. The condition can be rewritten as $\boldsymbol{\alpha}^*\boldsymbol{c}_{k^*}=-\sum_{j=1}^{M}\boldsymbol{\beta}^{*(j)}\boldsymbol{f}^{(j)}$. The prototype c_{k^*} scaled by α^* equals to the linear combination of negative samples. In other words, if the condition is true, the weights of models are unchanged due to zero gradients.

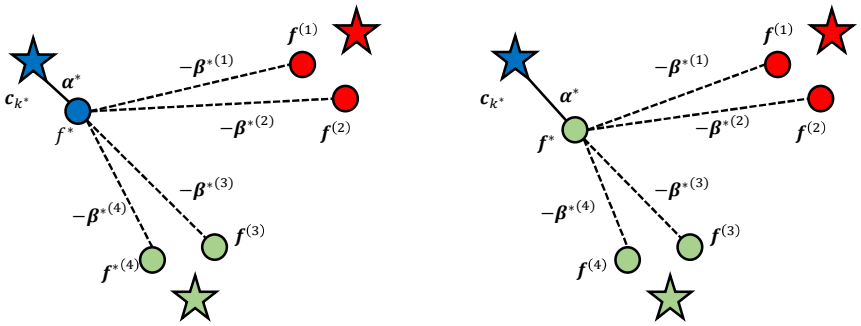

(a) (b)

Fig. 4. Two examples for zero gradients in feature space. (a) correct anchor assignment. (b) incorrect anchor assignment.

Fig. 4 illustrates two examples for zero gradients in feature space. Fig. 4 (a) shows correct anchor assignment that feature f^* (blue circle) is classified to the class with prototype c_{k^*} (blue star). This is a desired scenario where features are close to the correct prototypes and far away their corresponding negative samples.

Fig. 4 (b) exhibits incorrect anchor assignment that feature f^* (green circle) is misclassified to the class with prototype c_{k^*} (blue star). This situation is usually happened in early training iterations because the adaption between source and target domains is poorly performed. Additionally, Fig. 4 (b) depicts that the linear combination of negatives samples which include green points is equal to the scaled prototype $\alpha^* c_{k^*}$. However, this leads to an ambiguous problem that the scale factor $\boldsymbol{\alpha}^*$ is computed by the blue prototype and the green anchor rather than blue anchor. This situation implies zero gradients. This suffers from poor adaptions and zero gradients. Accordingly, the performance of the models is unchanged from now on because the update of weights of models is stuck. An observation can be found from the update rule of the gradient descent method in (12). $\boldsymbol{\theta}_{\mathcal{F}}$ is updated by two times gradients, $2\frac{\partial \ell_{cd}}{\partial f^*}\frac{\partial f^*}{\partial f}$. This results in that $\mathcal{F}$ converges very quickly. Unfortunately, this case makes the shortcomings mentioned above getting worse.

$$\boldsymbol{\theta}_{\mathcal{F}} \coloneqq \begin{cases} \boldsymbol{\theta}_{\mathcal{F}} - \eta\left(\frac{\partial \ell_{cd}}{\partial \boldsymbol{f}_1}\frac{\partial \boldsymbol{f}_1}{\partial \boldsymbol{f}} + \frac{\partial \ell_{cd}}{\partial \boldsymbol{f}_2}\frac{\partial \boldsymbol{f}_2}{\partial \boldsymbol{f}}\right), & \boldsymbol{f}_1 \neq \boldsymbol{f}_2 \\ \boldsymbol{\theta}_{\mathcal{F}} - 2\eta\frac{\partial \ell_{cd}}{\partial \boldsymbol{f}^*}\frac{\partial \boldsymbol{f}^*}{\partial \boldsymbol{f}}, & \boldsymbol{f}_1 = \boldsymbol{f}_2 = \boldsymbol{f}^* \end{cases} \tag{12}$$

This paper proposes a gradient scaling (GS) scheme to tackle the shortcomings by avoiding the occurrence of zero gradients. It can slow down the updating speed to effectively make $\mathcal{P}_1$ and $\mathcal{P}_2$ selecting distinct prototypes. The GS scheme is developed and represented in (13).

$$\boldsymbol{\theta}_{\mathcal{F}} \coloneqq \begin{cases} \boldsymbol{\theta}_{\mathcal{F}} - \lambda\eta\left(\frac{\partial \ell_{cd}}{\partial \boldsymbol{f}_1}\frac{\partial \boldsymbol{f}_1}{\partial \boldsymbol{f}} + \frac{\partial \ell_{cd}}{\partial \boldsymbol{f}_2}\frac{\partial \boldsymbol{f}_2}{\partial \boldsymbol{f}}\right), & \sum_{i=1}^{2}\left\|\boldsymbol{\alpha}\boldsymbol{c}_{k_i} + \sum_{j=1}^{M}\boldsymbol{\beta}^{(j)}\boldsymbol{f}^{(j)}\right\|_2 < \epsilon \\ \boldsymbol{\theta}_{\mathcal{F}} - \eta\left(\frac{\partial \ell_{cd}}{\partial \boldsymbol{f}_1}\frac{\partial \boldsymbol{f}_1}{\partial \boldsymbol{f}} + \frac{\partial \ell_{cd}}{\partial \boldsymbol{f}_2}\frac{\partial \boldsymbol{f}_2}{\partial \boldsymbol{f}}\right), & otherwise, \end{cases} \tag{13}$$

where $\|\cdot\|_2$ stands for l_2 norm, λ denotes a scaling factor of the gradients and ϵ refers to a threshold for the inequality condition, $\sum_{i=1}^{2}\left\|\boldsymbol{\alpha}\boldsymbol{c}_{k_i} + \sum_{j=1}^{M}\boldsymbol{\beta}^{(j)}\boldsymbol{f}^{(j)}\right\|_2 < \epsilon$. In the design of the GS scheme, when inequality holds, the gradients are scaled by λ and then are exploited to update $\boldsymbol{\theta}_{\mathcal{F}}$. This way can prevent too fast convergence to obtain zero gradients in early training iterations while updating $\boldsymbol{\theta}_{\mathcal{F}}$. Fig. 4 (b) illustrates the situation of occurring zero gradients.

The procedure of training the CBPUDA is given by **Algorithm 1**. The inputs of **Algorithm 1** include $\mathcal{D}_s$ and $\mathcal{D}_t$. **Algorithm 1** outputs three sets, $\boldsymbol{\theta}_{\mathcal{F}}$, $\boldsymbol{\theta}_{\mathcal{P}_1}$ and $\boldsymbol{\theta}_{\mathcal{P}_2}$, of weights for three trained models, $\mathcal{F}$, $\mathcal{P}_1$ and $\mathcal{P}_2$, respectively. Moreover, it also produces a set of weights for K prototypes, $\{\boldsymbol{c}_k\}_{k=1}^{K}$. In Step 1, $\boldsymbol{\theta}_{\mathcal{F}}$, $\boldsymbol{\theta}_{\mathcal{P}_1}$ and $\boldsymbol{\theta}_{\mathcal{P}_2}$ and $\{\boldsymbol{\theta}_{\boldsymbol{c}_k}\}_{k=1}^{K}$ are initialized. Then, $(\boldsymbol{x}^s, y^s)$ and $\boldsymbol{x}^t$ are randomly sampled from D_s and D_t, respectively. Steps 4-6 do the feed forward of $\mathcal{F}$, $\mathcal{P}_1$ and $\mathcal{P}_2$. Steps 7-8 compute ℓ_{cls} and ℓ_{cd} by (8) and (9), respectively. Subsequently, $\{\boldsymbol{c}_k\}_{k=1}^{K}$, $\boldsymbol{\theta}_{\mathcal{P}_1}$ and $\boldsymbol{\theta}_{\mathcal{P}_2}$ are updated in Step 9 by the backpropagation algorithm. Finally, $\boldsymbol{\theta}_{\mathcal{F}}$ is altered in Step

10 by the GS scheme in (13). Steps 3-10 are repeated for N_{iter} iterations.

Algorithm 1. The training algorithm of the CBPUDA
Input: Source image dataset D_s and target image dataset D_t;
Output: The weights of learned networks, $\boldsymbol{\theta}_{\mathcal{F}}$, $\boldsymbol{\theta}_{\mathcal{P}_1}$, $\boldsymbol{\theta}_{\mathcal{P}_2}$ and $\{\boldsymbol{\theta}_{\boldsymbol{c}_k}\}_{k=1}^{K}$;

1. Initialize network weights $\boldsymbol{\theta}_{\mathcal{F}}$, $\boldsymbol{\theta}_{\mathcal{P}_1}$, $\boldsymbol{\theta}_{\mathcal{P}_2}$ and $\{\boldsymbol{\theta}_{\boldsymbol{c}_k}\}_{k=1}^{K}$;
2. **For** iteration←1 to N_{iter} **do** //N_{iter} is maximal iteration
3. $(\boldsymbol{x}^s, y_s)\sim D_s$; $\boldsymbol{x}^t\sim D_t$;
4. $\boldsymbol{f}^s \leftarrow \mathcal{F}(\boldsymbol{x}^s)$; $\boldsymbol{f}^t \leftarrow \mathcal{F}(\boldsymbol{x}^t)$;
5. $\boldsymbol{f}_1^s \leftarrow \mathcal{P}_1(\boldsymbol{x}^s)$; $\boldsymbol{f}_1^t \leftarrow \mathcal{P}_1(\boldsymbol{x}^t)$;
6. $\boldsymbol{f}_2^s \leftarrow \mathcal{P}_2(\boldsymbol{x}^s)$; $\boldsymbol{f}_2^t \leftarrow \mathcal{P}_2(\boldsymbol{x}^t)$;
7. Compute the classification loss in (8);
8. Compute the contrastive discrepancy loss in (9);
9. Update $\{\boldsymbol{\theta}_{\boldsymbol{c}_k}\}_{k=1}^{K}$, $\boldsymbol{\theta}_{\mathcal{P}_1}$ and $\boldsymbol{\theta}_{\mathcal{P}_2}$ according to (8) and (9);
10 Update $\boldsymbol{\theta}_{\mathcal{F}}$ according to (8) and (9) with the updating rule in (13);
11 **end**

IV. Experimental Results

A. Datasets

Fig. 5 displays three UDA datasets, Office-31 [25], Office-Home [26] and Visda-2017 [27], which are employed in the experiments for the measurement of the performance of the CBPUDA. Fig. 5 (a) depicts that Office-31 dataset consists of three domains, Amazon (A), Web-cam (W) and DSLR (D). Each domain has 31 classes. In total, this dataset contains 4562 images. Fig. 5 (b) shows the Office-Home dataset which contains four domains, Art (A), Clipart (C), Product (P) and Real-World (R). Each domain has 65 classes. Totally, this dataset includes 15500 images. Fig. 5 (c) exhibits the Visa-2017 dataset which has two domains, Synthetic (S) and Real (R). Each domain has 12 classes. In total, this dataset comprises 280000 images. Note that S→T means source domain S is adapted to target domain R.

Each of three datasets, Plant Village (PV) [28], Plant Pathology 2020 (PP) [29] and Taiwan Dataset of Tomato Leaves (TDTL) [30], has very similar image contents. Consequently, identifying fine-grained image contents needs more classification ability. Fig. 6 depicts disease images of apple leaves in fine-grained UDA datasets. PV and PP are used as source and target datasets in this scenario, respectively. Apple leaf images in PV are selected in the experiments, which encompasses 1645 healthy, 275 rust and 630 scab images. PP comprises 516 healthy, 622 rust, 592 scab and 81 multiple diseases images for apple leaves. Fig. 7 illustrates disease images for tomato leaves in two fine-grained UDA datasets, PV and TDTL. Here, PV and TDTL are taken as source and target datasets, respectively. PV contains 1020 bacterial spot, 1272 healthy, 1528 late-blight, 762 mold and 1417 Septoria spot images for tomato leaves. TDTL consists of 704 bacterial spot, 678 healthy, 627 late-blight, 428 mold, 537 Septoria spot and 1256 powdery mildew images for tomato leaves. Because source and target domains require the same set of classes, some categories which are not in these three datasets are ignored.

Fig. 5. UDA datasets. (a) Office-31. (b) Office-home. (c) Visda-2017.

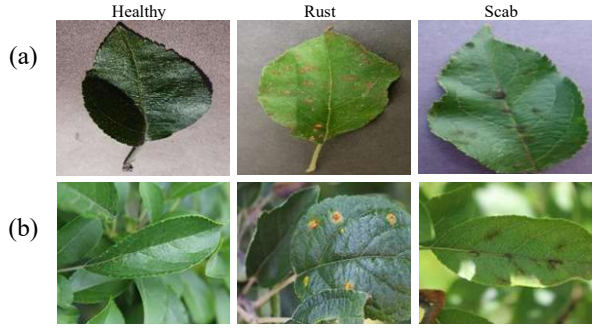

Fig. 6. Disease images for apple leaves in fine-grained UDA datasets. (a) PV and (b) PP.

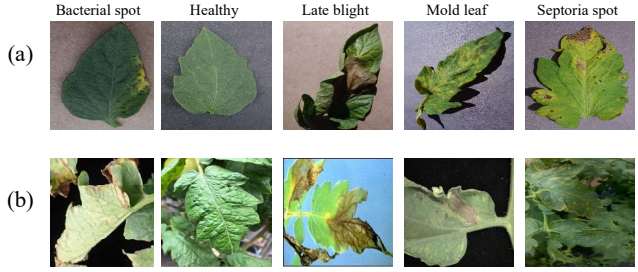

Fig. 7. Disease images for tomato leaves in fine-grained UDA datasets. (a) PP and (b) TDTL.

B. Experiment Settings

The CBPUDA is trained by the stochastic gradient decent (SGD) with a weight decay of 0.001. A learning rates for $\mathcal{F}$ is set to 0.0001 and the other for $\mathcal{P}_1$, $\mathcal{P}_2$ and $\{c_k\}_{k=1}^{K}$ is set to 0.005. The learning rate decay scheme can be found in [2] for updating $\mathcal{P}_1$, $\mathcal{P}_2$ and $\{c_k\}_{k=1}^{K}$. Moreover, the batch size for training the CBPUDA is of 36 for all datasets. In the GS scheme, λ and ϵ equal to 0.001 and 0.1, respectively. The temperature coefficient τ in (7) is assigned to 0.25 as default and the other values of τ are addressed in the experiments. The number of negative samples M is equivalent to 256 in the CD loss for all experiments. ResNet-50 is taken as $\mathcal{F}$ for training for all datasets except Visda-2017 which is involved in ResNet-101 [30]. Note that $\mathcal{F}$ is pretrained on ImageNet [31]. The CBPUDA is trained for 10000 iterations. The accuracy in (14) is exploited for quantitative evaluation.

$$Accuracy = \frac{card(\{\hat{y}^t | \hat{y}^t = y^t, \boldsymbol{x}^t \in D_t\})}{card(\{\boldsymbol{x}^t | \boldsymbol{x}^t \in D_t\})}, \qquad (14)$$

where $\hat{y}^t$ and $card(\cdot)$ represent the classification prediction and the cardinality of a set, respectively.

C. Quantitative Evaluation on UDA Datasets

Table I reports comparisons of performances of the CBPUDA and other baseline models. The best model is represented by bold and the second-best model is marked by bottom line in Table I. The symbol ↑ means boosting the offset in terms of accuracy when the performance of the CBPUDA is compared with that of the second-best model. The symbol ↓ denotes degrading the offset in terms of accuracy when the performance of the CBPUDA is compared with that of the best model. For example, the first (A→W) and the third column (W→A) in the last row in Table I show that ↑0.4 and ↓1.1. This indicates that the CBPUDA boosts the accuracy of the ATM about 0.4% and degrades the performance of the DSAN at 1.1% rate. Observing Table I, the performance of the CBPUDA is almost better than that of the baseline models except the case of W→A. The average accuracy increases 0.3%. Particularly, it achieves 100% on the case of D→W. Fig. 8 depicts the visualization of features on Office-31 for D→A. Figs. 8 (a)-(c) display the visualization of features for the BCDM, the CDAN and the CBPUDA, respectively. Obviously, the features generated by the CBPUDA have more discriminative clusters than that of the BCDM and the CDAN. This demonstrates the CBPUDA is effectively applied for learning the representation of the images.

Table II exhibits comparisons of performances of the CBPUDA and other baseline models on Office-Home. Compared to Office-31 that has 31 classes, there are 65 classes in Office-Home. Therefore, it is more difficult to perform the UDA on Office-Home. Despite Office-Home is more complicated, the CBPUDA receives 1.2% improvement comparing with the results of the second-best model in average accuracy. Especially, the CBPUDA boosts 1.8%, 1.7%, 2.9%, and 1.5% on four hard sub-tasks, A→C, P→A, P→C and R→C, respectively. Consequently, the CBPUDA is superior to other baseline models in the case of larger number of classes due to using the contrastive learning in the development of ℓ_{cd} in (7). In contrast, the MRAN, the DFA and the ATM do not take the relationship among features in the design of their loss functions. This leads to a limit of promoting their performance of the UDA on the dataset with large amount classes.

Table III presents comparisons of performances of the CBPUDA and other baseline models on Visda-2017. Because Visda-2017 is a large-scale dataset, it can be used to assess the model when massive images are available. The results of Table III reflect that the CBPUDA possesses better performance than the baseline models in the large-scale dataset scenario. The CBPUDA achieves 1.6% improvement than the DFCM in average accuracy. Since images in Visda-2017 have simple image contents with various poses of objects and clear backgrounds, the classification performances of models are almost very well except on Truck category due to large domain gap between S and R. In the first row of Table III, ResNet101 only gets 8.5% accuracy for Truck. In the seventh row of Table III, STAR with bi-classifier has 42.2% accuracy for Truck. Obviously, the CBPUDA achieves 50.7% accuracy, which outperforms STAR at 8.5% improvement.

TABLE I
COMPARISONS OF PERFORMANCES OF THE CBPUDA AND OTHER BASELINE MODELS ON OFFICE-31 IN TERMS OF ACCURACY (%)

Method	A→W	A→D	W→A	W→D	D→A	D→W	AVG
ResNet50	68.4	68.9	60.7	99.3	62.5	96.7	76.8
DAN [1]	80.5	78.6	62.8	99.6	63.6	97.1	80.4
DANN [2]	82.5	79.7	67.4	99.1	68.2	96.9	82.2
MRAN [12]	91.4	86.4	70.9	99.8	68.3	96.9	85.6
MCD [9]	88.6	92.2	69.7	100.0	69.5	98.5	86.5
JD-MMD [11]	91.2	86.9	71.8	100.0	70.5	97.6	86.3
DSAN [4]	93.6	90.2	**74.8**	100.0	73.5	98.3	88.4
SCA [16]	93.6	89.5	72.4	100.0	72.6	98.0	87.7
CDAN [6]	94.1	92.9	69.3	100.0	71.0	98.6	87.7
STAR [13]	92.6	93.2	70.8	100.0	71.4	98.7	87.8
DFA [3]	93.5	94.8	71.0	100.0	73.8	<u>99.4</u>	88.8
BCDM [10]	95.4	93.8	73.0	100.0	73.1	98.6	89.0
ATM [5]	<u>95.7</u>	<u>96.4</u>	73.5	<u>100.0</u>	<u>74.1</u>	99.3	<u>89.8</u>
CBPUDA	**96.1**	**96.6**	<u>73.7</u>	**100.0**	**74.3**	**100.0**	**90.1**
Offset	↑ 0.4	↑ 0.2	↓ 1.1	↑ 0.0	↑ 0.2	↑ 0.6	↑ 0.3

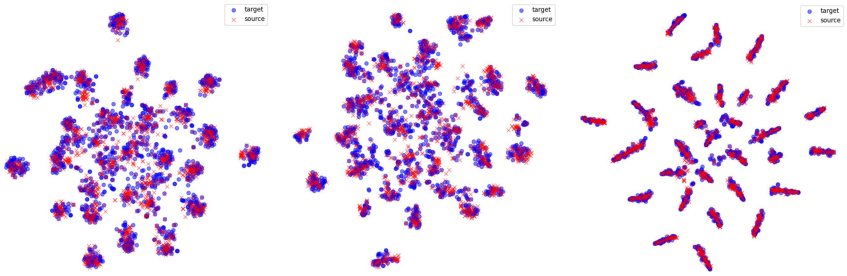

(a) (b) (c)

Fig. 8. Visualization of features of (a) BCDM, (b) CDAN and (c) CBPUDA on Office-31 for D→A using tSNE.

TABLE II
COMPARISONS OF PERFORMANCES OF THE CBPUDA AND OTHER BASELINE MODELS ON OFFICE-HOME IN TERMS OF ACCURACY (%)

Method	A→C	A→P	A→ R	C→ A	C→P	C→R	P→A	P→C	P→R	R→A	R→C	R→P	AVG
ResNet50	34.9	50.0	58.0	37.4	41.9	46.2	38.5	31.2	60.4	53.9	41.2	59.9	46.1
DAN [1]	43.6	57.0	67.9	45.8	56.5	60.4	44.0	43.6	67.7	63.1	51.5	74.3	56.3
DANN [2]	45.6	59.3	70.1	47.0	58.5	60.9	46.1	43.7	68.5	63.2	51.8	76.8	57.6
DSAN [4]	54.4	70.8	75.4	60.4	67.8	68.0	62.6	55.9	78.5	73.8	60.6	83.1	67.6
SCA [16]	46.7	64.6	71.3	53.1	65.3	65.2	54.6	47.2	72.7	68.2	56.0	80.2	62.1
CDAN [6]	50.7	70.6	76.0	57.6	70.0	70.0	57.4	50.9	77.3	70.9	56.7	81.6	65.8
MRAN [12]	53.8	68.6	75.0	57.3	66.1	68.2	57.3	51.4	75.9	70.4	60.0	82.2	66.2
DFA [3]	52.8	73.9	77.4	**66.5**	**72.9**	**73.6**	64.9	53.1	78.7	74.5	58.1	82.4	69.1
ATM [5]	52.4	72.6	78.0	61.1	72.0	72.6	59.5	52.0	79.1	73.3	58.9	83.4	67.9
CBPUDA	**55.6**	**74.3**	**78.5**	66.4	72.5	72.5	**66.6**	**56.0**	**79.5**	**75.6**	**61.5**	**84.0**	**70.3**
Offset	↑ 1.2	↑ 0.4	↑ 0.5	↓ 0.1	↓ 0.4	↓ 1.1	↑ 1.7	↑ 2.9	↑ 0.4	↑ 1.1	↑ 1.5	↑ 0.6	↑ 1.2

TABLE III
COMPARISONS OF PERFORMANCES OF THE CBPUDA AND OTHER BASELINE MODELS ON VISDA-2017 IN TERMS OF ACCURACY (%)

Method	Plane	Bicycle	Bus	Car	Horse	Knife	Mcycl	Person	Plant	Sktbrd	Train	Truck	AVG
ResNet101	55.1	53.3	61.9	59.1	80.6	17.9	79.7	31.2	81.0	26.5	73.5	8.5	52.4
DAN [1]	87.1	63.0	76.5	42.0	90.3	42.9	85.9	53.1	49.7	36.3	85.8	20.7	61.1
DANN [2]	81.9	77.7	82.8	44.3	81.2	29.5	65.1	28.6	51.9	54.6	82.8	7.8	57.4
MCD [9]	87.0	60.9	83.7	64.0	88.9	79.6	84.7	76.9	88.6	40.3	83.0	25.8	71.9
DSAN [4]	90.9	66.9	75.7	62.4	88.9	77.0	93.7	75.1	92.8	67.6	**89.1**	39.4	75.1
CDAN [6]	85.2	66.9	83.0	50.8	84.2	74.9	88.1	74.5	83.4	76.0	81.9	38.0	73.9
STAR [13]	95.0	84.0	84.6	73.0	91.6	91.8	85.9	78.4	94.4	84.7	87.0	42.2	82.7
BCDM [10]	95.1	87.6	81.2	73.2	92.7	95.4	86.9	82.5	95.1	84.8	88.1	39.5	83.4
DFCM [3]	95.4	88.8	83.2	**77.5**	92.6	**97.1**	88.9	**84.1**	94.9	86.2	88.6	42.1	85.0
CBPUDA	**96.9**	**88.8**	**86.7**	75.1	**94.2**	94.6	**95.1**	83.8	**97.0**	**87.4**	88.4	**50.7**	**86.6**
Offset	↑ 1.5	↑ 0.0	↑ 2.1	↓ 2.4	↑ 1.5	↓ 1.7	↑ 1.4	↓ 0.3	↑ 1.9	↑ 1.2	↓ 0.7	↑ 8.5	↑ 1.6

D. Quantitative Evaluation on Fine-Grained UDA Datasets

Table IV reports comparisons of performances of the CBPUDA and other baseline models on PV → PP. These comparisons focus on the quantitative evaluation results of the CBPUDA on fine-grained UDA datasets. The CBPUDA has outstanding performance more 27.34% average accuracy than that of the MRAN. Moreover, all categories of leaf diseases are almost perfectly recognized by the CBPUDA. In contrast, other models cannot well distinguish the image contents of subtle differences among diseases of apple leaves. The BCDM fails to identify rust apple leaves for getting 1.93% accuracy even though it performs well for identification on two categories, healthy and scab apple leaves. In addition, the MRAN just gets 52.57% accuracy.

Table V lists comparisons of performances of the CBPUDA and other baseline models on PV→TDTL. The results of Table V show the UDA models are hard to perform well on PV→PP because many disease images in the TDTL are almost identical. The CBPUDA can obtain the best performance among the baseline models. It improves the performance of the MRAN at increasing 7.96% average accuracy. Moreover, the CBPUDA effectively boosts three hard categories, bacterial spot, late-blight, and mold for 7.24%, 5.38% and 5.40%, respectively. The conditional UDA models in Table V except the CBPUDA all are unstable for fine-grained UDA datasets. The BCDM poorly identifies healthy category in the TDTL as it merely gets 29.65% accuracy which is much less

than 70.61% ResNet50 acquires. The DSAN almost cannot recognize Septoria spot category in the TDTL, which just gains 0.29% accuracy.

TABLE IV
COMPARISONS OF PERFORMANCES OF THE CBPUDA AND OTHER BASELINE MODELS ON PV→PP IN TERMS OF ACCURACY (%)

Method	Healthy	Rust	Scab	AVG
ResNet50	11.02	24.10	79.54	39.27
DAN [1]	11.84	34.99	89.02	48.89
DANN [2]	28.71	30.26	85.12	50.04
DSAN [4]	51.24	35.42	83.96	56.41
MRAN [12]	70.87	52.57	81.28	67.45
BCDM [10]	**97.09**	1.93	88.51	59.65
CBPUDA	94.96	**92.92**	**96.79**	**94.79**
Offset	↓ 2.13	↑ 37.11	↑ 7.77	↑ 27.34

Table V
COMPARISONS OF PERFORMANCES OF THE CBPUDA AND OTHER BASELINE MODELS ON PV→TDTL IN TERMS OF ACCURACY (%)

Method	Bacterial spot	Healthy	Late blight	Mold	Septoria spot	AVG
ResNet50	5.34	70.61	1.25	25.03	6.36	21.46
DSAN [4]	10.51	92.03	1.64	29.61	0.29	27.57
DANN [2]	8.24	86.92	3.50	38.73	4.13	28.71
DAN [1]	12.22	83.41	0.93	38.18	67.11	42.80
MRAN [12]	18.47	75.92	2.11	33.15	**78.64**	44.86
BCDM [10]	15.48	29.65	7.94	40.22	5.28	34.03
CBPUDA	**25.71**	**99.71**	**13.32**	**45.62**	65.71	**52.82**
Offset	↑ 7.24	↑ 7.68	↑ 5.38	↑ 5.40	↓ 1.40	↑ 7.96

E. Analysis of the Contrastive Discrepancy Loss

To examine the effectiveness of the GS scheme and its performance with τ, τ is individually set to 0.25, 0.5, 0.75 and 1.0 in the experiments. For each case, training the CBPUDA with (w) and without (w/o) are evaluated by observing the learning curves as shown in Fig. 9. Fig. 9 (a) conveys two learning curves for training the CBPUDA with and without using the GS scheme while $\tau = 0.25$. To recall the formulation of the gradients for ℓ_{cd} in (11), $\frac{\partial \ell_{cd}}{\partial f}$ is scaled by the $\frac{1}{\tau}$. Therefore, Fig. 9 (a) illustrates that the learning curve during training the CBPUDA without the GS scheme, which is almost stuck after a few iterations. This results in that the CBPUDA gets poor performance due to no scaling the large gradients using (13). That is, it is easy to stuck on zero gradients because the large gradients cause updating weights so fast. Conversely, the learning curve during training the CBPUDA with the GS scheme shows stable with slightly increasing the performance as more iterations. Figs. (b)-(d) express learning curves during training the CBPUDA in three cases of large τ for 0.5, 0.75 and 1.0, respectively. Because $\frac{\partial \ell_{cd}}{\partial f}$ is scaled by $\frac{1}{\tau}$, increasing the value of τ can mitigate the situation of updating weights by gradients not so fast. Namely, two of their learning curves during training the CBPUDA without the GS scheme are almost getting overlapped with learning curves with the GS scheme when τ goes larger. In other words, it means updating the weights of the CBPUDA by less gradients throughout all iterations.

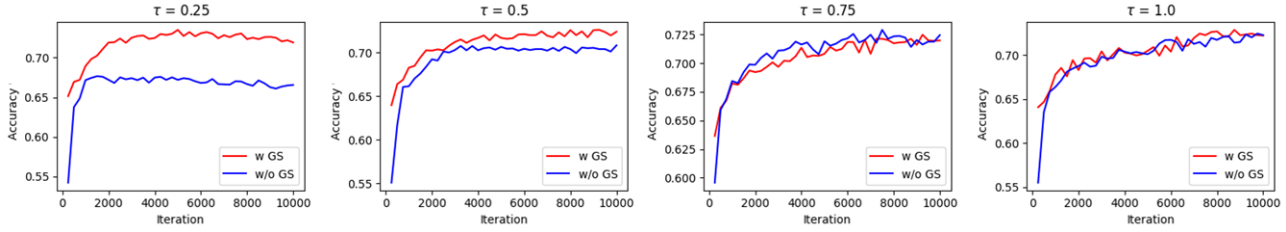

(a) (b) (c) (d)

Fig. 9. Comparisons of the learning curves of training the CBPUDA w and w/o GS for the cases, (a) $\tau = 0.25$, (b) $\tau = 0.5$, (c) $\tau = 0.75$ and (d) $\tau = 1.0$ on Office-31 for D→A.

However, although assigning τ with larger value in ℓ_{cd} can mitigate unstable training, less τ for contrastive learning introduces large penalty on hard negative samples. It makes features more discriminative due to negative features far away from anchor features [34]. Accordingly, using large τ has a difficulty to obtain nearly optimal performance of the CBPUDA. Fig. 10 draws comparisons of the learning curves during training the CBPUDA with the GS scheme in the cases of $\tau = 0.25, 0.5, 0.75$, and 1.0. The blue curve ($\tau = 0.25$) outperforms other curves ($\tau = 0.5, 0.75, 1.0$). This result demonstrates that training the CBPUDA with the GS scheme accompanying with less τ can take the advantage of the characteristics of contrastive learning. Moreover, Figs. 11(a)-(d) depict the visualization for features generated by the CBPUDA exploiting $\tau = 0.25, 0.5, 0.75$ and 1.0, respectively. Obviously, features on $\tau = 0.25$ are more significantly discriminative than others.

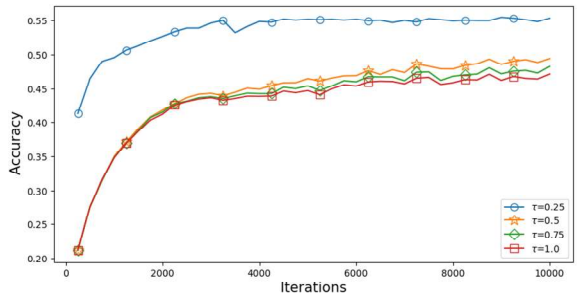

Fig. 10. Comparisons of the learning curves of training the CBPUDA with GS in the cases of $\tau = 0.25, 0.5, 0.75, 1.0$ on Office-Home for A→C.

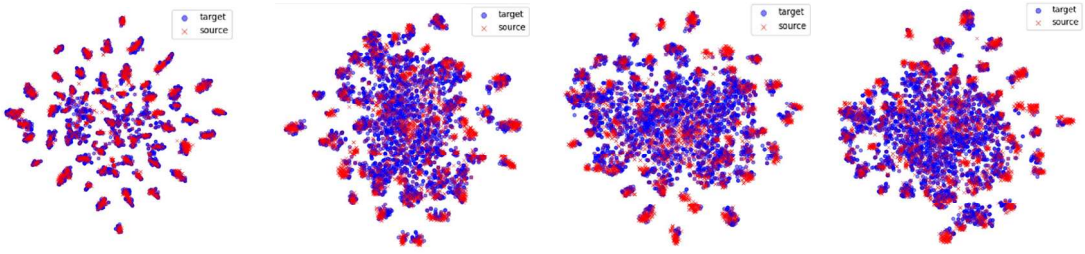

(a) (b) (c) (d)

Fig. 11. Visualization for features generated by the CBPUDA with (a) $\tau = 0.25$, (b) $\tau = 0.5$, (c) $\tau = 0.75$ and (d) $\tau = 1.0$ on Office-Home for A→C using tSNE.

Let Γ and Φ be two loss functions, which are specified by $-\log\left(e^{f_1^T c_{k_1}+f_2^T c_{k_2}}\right)$ and $\log\left(e^{f_1^T c_{k_1}+f_2^T c_{k_2}}+\sum_{j=1}^{M}\sum_{j'=1}^{M} 1_{y^{(j)}\neq k_1, y^{(j')}\neq k_2} e^{f_1^T f^{(j)}+f_2^T f^{(j')}}\right)$, respectively. Fig. 12 draws the learning curves for ℓ_{cd}, Γ and Φ on Office-Home. Γ expresses the loss function for merely using anchor and positive samples in (7). Φ stands for the loss function for including anchor and negative samples but only the denominator term in (7). Observing Fig. 12, the results point to that using ℓ_{cd} can obtain the better performance than using other two loss functions, Γ and Φ. Moreover, the performances of using ℓ_{cd} to train the CBPUDA are slightly better than using Γ on seven sub-tasks, A→P, A→R, C→A, C→P, C→R, P→R and R→P. Using ℓ_{cd} is significantly superior to that using Γ on five sub-tasks, A→C, P→A, P→C, R→A and R→C. Hence, involving negative samples can powerfully improve the performance of just using prototypes in loss function ℓ_{cd} on some hard UDA sub-tasks. In addition, the performance of using Φ to train the CBPUDA is acceptable on A→R, which is slightly less than using ℓ_{cd}. This result shows training an UDA model without updating prototypes still works for easy sub-tasks. Although using Φ to perform the training of an UDA model is acceptable on A→R, it cannot be well trained and causes overfitting on other sub-tasks harder than A→R. Therefore, training the CBPUDA still needs the prototypes to pull the features into the clusters they belong to while processing other sub-tasks harder than A→R. Figs. 12 (a)-(c) exhibits the visualizations for features produced by the CBPUDA utilizing ℓ_{cd}, Γ and Φ, respectively. The results reflect that using ℓ_{cd} makes the features more discriminative than using Γ and Φ. Moreover, the features in Fig. 13 (b) are more distinguishable than the features in Fig. 14 (c) because optimizing Γ can pull the features to prototypes but Φ does not.

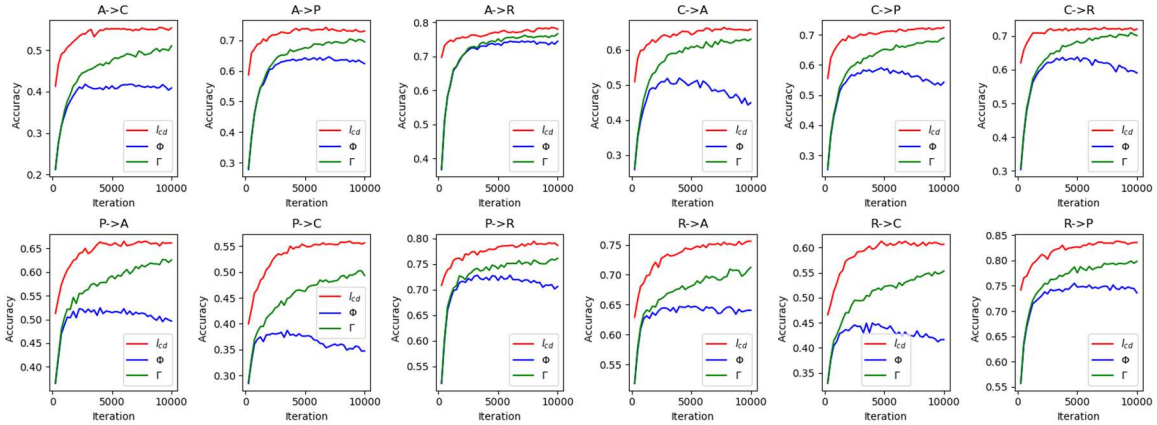

Fig. 12. Learning curves of using ℓ_{cd}, Γ and Φ on Office-Home.

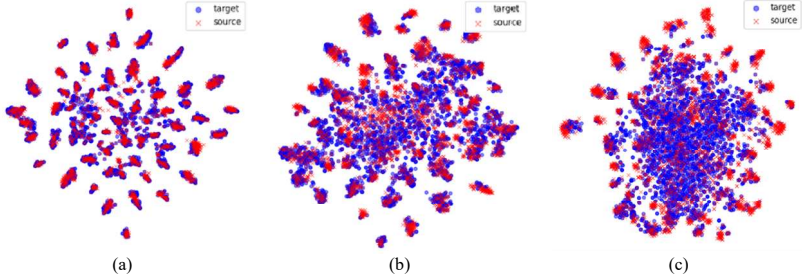

(a) (b) (c)

Fig. 13. Visualizations for the features of training the CBPUDA with (a) ℓ_{cd}, (b) Γ and (c) Φ. on Office-Home for A→C.

V. Conclusion

This paper has proposed a novel approach for the UDA, the CBPUDA, which leverages the CBP in the design of the CBPUDA to significantly reduce the generation of ambiguous features during classification. Two properties have been derived in this paper, an upper bound (CD loss) of the joint prediction entropy and the analysis of the gradients for the CD loss. The upper bound is derived by involving contrastive learning and bi-classifier. Additionally, the GS scheme has been devised in this paper to tackle the instable situation of the CD loss because the CD loss is developed by contrastive learning and adversarial learning. By combining the CD loss with the GS scheme in the design of the CBPUDA, the FE of the CBPUDA achieves more compact intra-class features and distinct inter-class features. Notably, the CBPUDA differs from traditional bi-classifier methods in that it employs the CBP to map input features (generated by the FE) into two distinct features. This helps to train the CBPUDA adversarially to refine decision boundaries and empower the CBPUDA with robust classification capabilities.

Experimental results demonstrates that the CBPUDA is superior to the baseline models across various UDA tasks in consideration of this paper. The successful discrimination for fine-grained image contents and the advantageous properties of the CD loss further highlights the potential of the CBPUDA for solving complex UDA challenges. Therefore, the CBPUUDA can be applied in real-world applications. In the future research, the CBPUDA can be further improved by developing a simplified version of the CD loss, optimizing the negative sampling strategy, and refining the GS conditions.

Appendix A
Proof of Property I

The product of two predictions can be written in (15) by plugging $p_i(y = k_i|\boldsymbol{x})$ in (6) into (3).

$$p_1(y=k_1|\boldsymbol{x})p_2(y=k_2|\boldsymbol{x}) = \frac{e^{\boldsymbol{f}_1^T\boldsymbol{c}_{k_1}}}{\sum_k e^{\boldsymbol{f}_1^T\boldsymbol{c}_k}}\frac{e^{\boldsymbol{f}_2^T\boldsymbol{c}_{k_2}}}{\sum_{k'} e^{\boldsymbol{f}_2^T\boldsymbol{c}_{k'}}} = \frac{e^{\boldsymbol{f}_1^T\boldsymbol{c}_{k_1}}e^{\boldsymbol{f}_2^T\boldsymbol{c}_{k_2}}}{\sum_k e^{\boldsymbol{f}_1^T\boldsymbol{c}_k}\sum_{k'} e^{\boldsymbol{f}_2^T\boldsymbol{c}_{k'}}} = \frac{e^{\boldsymbol{f}_1^T\boldsymbol{c}_{k_1}}e^{\boldsymbol{f}_2^T\boldsymbol{c}_{k_2}}}{e^{\boldsymbol{f}_1^T\boldsymbol{c}_{k_1}}e^{\boldsymbol{f}_2^T\boldsymbol{c}_{k_2}} + \sum_{k\neq k_1,k'\neq k_2} e^{\boldsymbol{f}_1^T\boldsymbol{c}_k+\boldsymbol{f}_2^T\boldsymbol{c}_{k'}}}. \quad (15)$$

The component in (15), $\sum_{k\neq k_1,k'\neq k_2} e^{\boldsymbol{f}_1^T\boldsymbol{c}_k+\boldsymbol{f}_2^T\boldsymbol{c}_{k'}}$, can be further derived using the definition of prototypes in (5) and *Jensen Inequality* [35] to obtain the upper bound of $\sum_{k\neq k_i} e^{\boldsymbol{f}_i^T\boldsymbol{c}_k}$ in (16).

$$\begin{aligned}\sum_{k\neq k_i} e^{\boldsymbol{f}_i^T\boldsymbol{c}_k} &= \sum_{k\neq k_i} e^{\boldsymbol{f}_i^T\mathbb{E}[\boldsymbol{f}|y=k]} \\ &\leq \sum_{k\neq k_i}\mathbb{E}\left[e^{\boldsymbol{f}_i^T\boldsymbol{f}}|y=k\right] \\ &= K\mathbb{E}\left[e^{\boldsymbol{f}_i^T\boldsymbol{f}}|y\neq k_i\right] \\ &\approx \frac{K}{M}\sum_{j=1}^{M} 1_{y^{(j)}\neq k_i} e^{\boldsymbol{f}_i^T\boldsymbol{f}^{(j)}} \\ &\leq \sum_{j=1}^{M} 1_{y^{(j)}\neq k_i} e^{\boldsymbol{f}_i^T\boldsymbol{f}^{(j)}}. \end{aligned} \quad (16)$$

Replacing the right term in the last inequality in (16) with $\sum_{k\neq k_1,k'\neq k_2} e^{\boldsymbol{f}_1^T\boldsymbol{c}_k+\boldsymbol{f}_2^T\boldsymbol{c}_{k'}}$ in (15), the inequality of the product between the predictions of two classifiers can be formulated in (17). Finally, (18) conveys that the contrastive discrepancy loss is the upper bound of the joint prediction entropy.

$$\frac{e^{\boldsymbol{f}_1^T\boldsymbol{c}_{k_1}}}{\sum_k e^{\boldsymbol{f}_1^T\boldsymbol{c}_k}}\frac{e^{\boldsymbol{f}_2^T\boldsymbol{c}_{k_2}}}{\sum_{k'} e^{\boldsymbol{f}_2^T\boldsymbol{c}_{k'}}} \geq \frac{e^{(\boldsymbol{f}_1^T\boldsymbol{c}_{k_1}+\boldsymbol{f}_2^T\boldsymbol{c}_{k_2})/\tau}}{e^{(\boldsymbol{f}_1^T\boldsymbol{c}_{k_1}+\boldsymbol{f}_2^T\boldsymbol{c}_{k_2})/\tau} + \sum_{j=1}^{M}\sum_{j'=1}^{M} 1_{y^{(j)}\neq k_1, y^{(j')}\neq k_2} e^{\left(\boldsymbol{f}_1^T\boldsymbol{f}^{(j)}+\boldsymbol{f}_2^T\boldsymbol{f}^{(j')}\right)/\tau}} \quad (17)$$

$$H(p_1,p_2) \leq \mathbb{E}_{x^t\sim D_t,\{x_j\}_{j=1}^{M}\sim\{D_s\cup D_t\}}\left[-\log\frac{e^{(\boldsymbol{f}_1^T\boldsymbol{c}_{k_1}+\boldsymbol{f}_2^T\boldsymbol{c}_{k_2})/\tau}}{e^{(\boldsymbol{f}_1^T\boldsymbol{c}_{k_1}+\boldsymbol{f}_2^T\boldsymbol{c}_{k_2})/\tau} + \sum_{j=1}^{M}\sum_{j'=1}^{M} 1_{y^{(j)}\neq k_1, y^{(j')}\neq k_2} e^{\left(\boldsymbol{f}_1^T\boldsymbol{f}^{(j)}+\boldsymbol{f}_2^T\boldsymbol{f}^{(j')}\right)/\tau}}\right] \quad (18)$$

Appendix B
Proof of Property II

Assume $\boldsymbol{\alpha}^*\boldsymbol{c}_{k^*} = 0$, we have the results of (19),

$$\boldsymbol{\alpha}^*\boldsymbol{c}_{k^*} = 0 \Rightarrow -1 + \frac{1}{\boldsymbol{B}^*}e^{\frac{2\boldsymbol{f}^{*T}\boldsymbol{c}_{k^*}}{\tau}} = 0 \Longrightarrow \boldsymbol{B}^* = e^{\frac{2\boldsymbol{f}^{*T}\boldsymbol{c}_{k^*}}{\tau}}. \quad (19)$$

But $\sum_{j=1}^{M}\sum_{j'=1}^{M} 1_{y^{(j)}\neq k^*\neq y^{(j')}} e^{\frac{\boldsymbol{f}^{*T}\left(\boldsymbol{f}^{(j)}+\boldsymbol{f}^{(j')}\right)}{\tau}} > 0$ in (7), therefore we have $\boldsymbol{\alpha}^*\boldsymbol{c}_{k^*} \neq 0$ as shown in (20).

$$\boldsymbol{B}^* = e^{\frac{2\boldsymbol{f}^{*T}\boldsymbol{c}_{k^*}}{\tau}} + \sum_{j=1}^{M}\sum_{j'=1}^{M} 1_{y^{(j)}\neq k^*\neq y^{(j')}} e^{\frac{\boldsymbol{f}^{*T}\left(\boldsymbol{f}^{(j)}+\boldsymbol{f}^{(j')}\right)}{\tau}} \neq e^{\frac{2\boldsymbol{f}^{*T}\boldsymbol{c}_{k^*}}{\tau}} \Rightarrow \boldsymbol{\alpha}^*\boldsymbol{c}_{k^*} \neq 0. \quad (20)$$

Because $\frac{\partial \ell_{cd}}{\partial \boldsymbol{f}^*}$ is the summation of $\boldsymbol{\alpha}^* \boldsymbol{c}_{k^*}$ and $\sum_{j=1}^{M} \boldsymbol{\beta}^{*(j)} \boldsymbol{f}^{(j)}$ in (11), thus $\sum_{j=1}^{M} \boldsymbol{\beta}^{*(j)} \boldsymbol{f}^{(j)} \neq 0$. Accordingly, $(\boldsymbol{\alpha}^* \boldsymbol{c}_{k^*})\left(\sum_{j=1}^{M} \boldsymbol{\beta}^{*(j)} \boldsymbol{f}^{(j)}\right) \neq 0$.

REFERENCES

[1] M. Long, Y. Cao, J. Wang, and M. Jordan, "Learning transferable features with deep adaptation networks," in Proceedings of the International Conference on Machine Learning, Jun. 2015, pp. 97-105.

[2] Y. Ganin and V. Lempitsky, "Unsupervised domain adaptation by backpropagation," in Proceedings of the International Conference on Machine Learning, Jun. 2015, pp. 1180-1189.

[3] J. Wang, J. Chen, J. Lin, L. Sigal, and C. W. de Silva, "Discriminative feature alignment: Improving transferability of unsupervised domain adaptation by Gaussian-guided latent alignment," Pattern Recognition, vol. 116, pp. 107943, 2021.

[4] Y. Zhu, F. Zhuang, J. Wang, G. Ke, J. Chen, J. Bian, et al., "Deep subdomain adaptation network for image classification," IEEE Transactions on Neural Networks and Learning Systems, vol. 32, no. 4, pp. 1713-1722, 2020.

[5] J. Li, E. Chen, Z. Ding, L. Zhu, K. Lu, and H. T. Shen, "Maximum density divergence for domain adaptation," IEEE Transactions on Pattern Analysis and Machine Intelligence, vol. 43, no. 11, pp. 3918-3930, 2020.

[6] M. Long, Z. Cao, J. Wang, and M. I. Jordan, "Conditional adversarial domain adaptation," in Advances in Neural Information Processing Systems, vol. 31, 2018.

[7] H. Zhang, J. Tang, Y. Cao, Y. Chen, Y. Wang, and Q. J. Wu, "Cycle Consistency Based Pseudo Label and Fine Alignment for Unsupervised Domain Adaptation," IEEE Transactions on Multimedia, 2022.

[8] M. Wang and W. Deng, "Cycle label-consistent networks for unsupervised domain adaptation," Neurocomputing, vol. 422, pp. 186-199, 2021.

[9] K. Saito, K. Watanabe, Y. Ushiku, and T. Harada, "Maximum classifier discrepancy for unsupervised domain adaptation," in Proceedings of the IEEE Conference on Computer Vision and Pattern Recognition, Jun. 2018, pp. 3723-3732.

[10] S. Li, F. Lv, B. Xie, C. H. Liu, J. Liang, and C. Qin, "Bi-classifier determinacy maximization for unsupervised domain adaptation," in Proceedings of the AAAI Conference on Artificial Intelligence, vol. 35, no. 10, May 2021, pp. 8455-8464.

[11] Q. Tian, J. Zhou, and Y. Chu, "Joint bi-adversarial learning for unsupervised domain adaptation," Knowledge-Based Systems, vol. 248, p. 108903, 2022.

[12] Y. Zhu, F. Zhuang, J. Wang, J. Chen, Z. Shi, W. Wu, et al., "Multi-representation adaptation network for cross-domain image classification," Neural Networks, vol. 119, pp. 214-221, 2019.

[13] Z. Lu, Y. Yang, X. Zhu, C. Liu, Y. Z. Song, and T. Xiang, "Stochastic classifiers for unsupervised domain adaptation," in Proceedings of the IEEE/CVF Conference on Computer Vision and Pattern Recognition, Jun. 2020, pp. 9111-9120.

[14] Z. Yu, J. Li, L. Zhu, K. Lu, and H. T. Shen, "Uneven Bi-Classifier Learning for Domain Adaptation," IEEE Transactions on Circuits and Systems for Video Technology, 2022.

[15] M. Xu, J. Zhang, B. Ni, T. Li, C. Wang, Q. Tian, and W. Zhang, "Adversarial domain adaptation with domain mixup," in Proceedings of the AAAI Conference on Artificial Intelligence, vol. 34, no. 04, Apr. 2020, pp. 6502-6509.

[16] W. Deng, L. Zheng, Y. Sun, and J. Jiao, "Rethinking triplet loss for domain adaptation," IEEE Transactions on Circuits and Systems for Video Technology, vol. 31, no. 1, pp. 29-37, 2020.

[17] H. Wang, J. Tian, S. Li, H. Zhao, F. Wu, and X. Li, "Structure-conditioned adversarial learning for unsupervised domain adaptation," Neurocomputing, vol. 497, pp. 216-226, 2022.

[18] A. van den Oord, Y. Li, and O. Vinyals, "Representation learning with contrastive predictive coding," arXiv preprint arXiv:1807.03748, 2018.

[19] T. Chen, S. Kornblith, M. Norouzi, and G. Hinton, "A simple framework for contrastive learning of visual representations," in Proceedings of the International Conference on Machine Learning, Nov. 2020, pp. 1597-1607.

[20] P. Khosla, P. Teterwak, C. Wang, A. Sarna, Y. Tian, P. Isola, et al., "Supervised contrastive learning," in Advances in Neural Information Processing Systems, vol. 33, 2020, pp. 18661-18673.

[21] T. Park, A. A. Efros, R. Zhang, and J. Y. Zhu, "Contrastive learning for unpaired image-to-image translation," in Computer Vision–ECCV 2020, Aug. 2020, pp. 319-345.

[22] M. Kang and J. Park, "Contragan: Contrastive learning for conditional image generation," in Advances in Neural Information Processing Systems, vol. 33, 2020, pp. 21357-21369.

[23] M. Kang, W. Shim, M. Cho, and J. Park, "Rebooting acgan: Auxiliary classifier gans with stable training," in Advances in Neural Information Processing Systems, vol. 34, 2021, pp. 23505-23518.

[24] A. Odena, C. Olah, and J. Shlens, "Conditional image synthesis with auxiliary classifier gans," in International Conference on Machine Learning, Jul. 2017, pp. 2642-2651.

[25] K. Saenko, B. Kulis, M. Fritz, and T. Darrell, "Adapting visual category models to new domains," in Computer Vision–ECCV 2010, Sep. 2010, pp. 213-226.

[26] H. Venkateswara, J. Eusebio, S. Chakraborty, and S. Panchanathan, "Deep hashing network for unsupervised domain adaptation," in Proceedings of the IEEE Conference on Computer Vision and Pattern Recognition, Jun. 2017, pp. 5018-5027.

[27] X. Peng, B. Usman, N. Kaushik, J. Hoffman, D. Wang, and K. Saenko, "Visda: The visual domain adaptation challenge," arXiv preprint arXiv:1710.06924, 2017.

[28] D. Hughes and M. Salathé, "An open access repository of images on plant health to enable the development of mobile disease diagnostics," arXiv preprint arXiv:1511.08060, 2015.

[29] R. Thapa, N. Snavely, S. Belongie, and A. Khan, "The plant pathology 2020 challenge dataset to classify foliar disease of apples," arXiv preprint arXiv:2004.11958, 2020.

[30] K. He, X. Zhang, S. Ren, and J. Sun, "Deep residual learning for image recognition," in Proceedings of the IEEE Conference on Computer Vision and Pattern Recognition, Jun. 2016, pp. 770-778.

[31] J. Deng, W. Dong, R. Socher, L. J. Li, K. Li, and L. Fei-Fei, "Imagenet: A large-scale hierarchical image database," in 2009 IEEE conference on computer vision and pattern recognition, Jun. 2009, pp. 248-255.

[32] I. Goodfellow, J. Pouget-Abadie, M. Mirza, B. Xu, D. Warde-Farley, S. Ozair, et al., "Generative adversarial nets," in Advances in Neural Information Processing Systems, vol. 27, 2014.

[33] L. Van der Maaten and G. Hinton, "Visualizing data using t-SNE," Journal of Machine Learning Research, vol. 9, no. 11.

[34] F. Wang and H. Liu, "Understanding the behaviour of contrastive loss," in Proceedings of the IEEE/CVF conference on computer vision and pattern recognition, Jun. 2021, pp. 2495-2504.

[35] J. L. W. V. Jensen, "Sur les fonctions convexes et les inégalités entre les valeurs moyennes," Acta mathematica, vol. 30, no. 1, pp. 175-193, 1906.